Mechanical Resonance and Damping in a Hacksaw Blade Oscillator

Ahilan Kumaresan[a]

Physics Department, Simon Fraser University, Burnaby, BC, Canada

(Dated: March 25, 2025)

[a] Lab partner: Alakhdeep Singh Sandhu

Harmonic oscillators are fundamental to physics and engineering, appearing in systems from simple pendulums to advanced vibrational analysis in materials science. Understanding resonance and damping in oscillatory systems is critical in designing structures, vehicles, and electronic circuits, where unwanted resonance can lead to catastrophic failure or where controlled damping is used to absorb energy [1, 2]. To better understand the underlying principles in harmonic oscillations, I investigate a damped simple harmonic oscillator by analyzing a hacksaw blade's forced and free oscillations. A hacksaw blade, serving as a cantilever, is chosen for its uniform elasticity and high-quality factor under minimal damping, making it suitable for studying resonance. The primary goals are

1. Measure how the frequency response depends on damping,
2. Extract parameters such as natural frequency, damping coefficient, and quality factor from forced and free oscillations,
3. Test how well a linear damped simple harmonic oscillator model describes the collected data.

A sinusoidal input voltage $V_{\text{in}}(t)$ is generated by a function generator [5] and applied to a small mechanical driver to drive the system. This driver induces vibrations in a cantilevered hacksaw blade, which serves as the oscillating system under study.

The blade's motion is measured using an analog accelerometer [3] mounted near its free end. The accelerometer produces a voltage signal $V_{\text{acc}}(t)$, which is linearly proportional to the instantaneous acceleration $a(t)$. Both the input $V_{\text{in}}(t)$ and output $V_{\text{acc}}(t)$ signals are simultaneously acquired by a data acquisition device (DAQ) [4] and recorded on a computer.

To convert the accelerometer output into physical acceleration units, a two-point calibration was performed by orienting the sensor at 0g and +1g. The corresponding

voltages were $V_0 = 1.47080$ V and $V_{+g} = 1.77318$ V, yielding the calibration relation

$$a(V) = g \cdot \frac{V - V_0}{V_{+g} - V_0}$$

with a gain of approximately $\Delta A \approx 32.43$ m/s^2/V. This result was cross-validated with the -1g orientation, and the estimated statistical uncertainty in the gain is ~ 0.5 m/s^2/V. Systematic uncertainties are assumed negligible within the calibration range [6].

Damping in the system is introduced using a permanent magnet placed above the blade without contact. By varying the vertical separation between the magnet and a fixed copper plate, we control the level of eddy-current damping in a non-invasive manner [2]. We tested three damping configurations – minimal, moderate, and maximal – by placing the magnet far, intermediate distance, and close.

To probe the system's resonance behavior, we perform a frequency sweep of the input signal $V_{\text{in}}(t)$ from 10–30 Hz. For each drive frequency, the corresponding response $V_{\text{acc}}(t)$ is recorded, and the software computes the amplitude ratio $V_{\text{acc}}/V_{\text{in}}$. This produces the system's amplitude and phase response curves as functions of frequency. Additionally, after switching off the drive, free-decay signals are recorded. These transients provide an independent estimate of the damping parameters and serve as a consistency check against the frequency-domain analysis.

We model the system as a damped, driven harmonic oscillator governed by Newton's second law. The restoring force is given by Hooke's law ($F = -kx$), assuming linear elasticity and the damping force is proportional to velocity. The system is assumed to oscillate in a single dominant mode with linear damping, and the external driving force is sinusoidal $F(t) = F_0 e^{i\omega t}$. Giving the equation of motion

$$\ddot{x} + 2\gamma\dot{x} + \omega_0^2 x = \frac{F_0}{m} e^{i\omega t} \tag{1}$$

where m is the effective mass, $\omega_0 = \sqrt{k/m}$ is the natural angular frequency, and

γ is the damping coefficient [2]. The general solution consists of a transient term, which decays over time, and a steady-state oscillation at the drive frequency ω, with amplitude and phase determined by both the damping and the detuning $\omega - \omega_0$. The sharpness of the resonance peak and the system's ability to store energy are characterized by the quality factor

$$Q = \frac{\omega_0}{2\gamma} \tag{2}$$

This dimensionless quantity represents the ratio of energy stored to energy lost per cycle. A large Q implies low damping and a narrow resonance peak, meaning the system oscillates for many cycles before losing energy. Conversely, a small Q indicates stronger damping and faster energy loss. In driven systems, Q controls both the width and height of the resonance response, making it a key parameter in quantifying how selective the system is to the drive frequency in our experiment.

Steady-State (Forced) Oscillations. In our system, the mechanical shaker is driven by V_{in}, which controls the applied force amplitude. While the exact force F_0 is not measured, it is assumed proportional to V_{in}, so the term F_0/m is absorbed into a scale constant C.

The steady-state amplitude of the acceleration response is measured via the ratio $V_{\text{acc}}/V_{\text{in}}$, modeled by

$$\frac{V_{\text{acc}}}{V_{\text{in}}}(\omega) = C \cdot \frac{\omega^2}{\sqrt{(\omega^2 - \omega_0^2)^2 + (2\gamma\omega)^2}} \tag{3}$$

which peaks at resonance and decreases away from it [2, 7]. The phase shift is

$$\phi = \tan^{-1}\left(\frac{2\gamma\omega}{\omega^2 - \omega_0^2}\right) \tag{4}$$

In addition to steady-state measurements, analyzing the transient decay after switching off the drive provides an independent method to extract the system's natural frequency ω_0 and damping coefficient γ. While the forced response is influenced

by the external driving frequency, the free-decay behavior reflects the system's intrinsic properties without external perturbations. Studying this regime allows us to test whether a linear damped harmonic oscillator model can fully describe the dissipation in the system. Furthermore, comparing damping parameters obtained from both methods helps identify non-ideal effects such as friction or nonlinear drag that may not be captured in the steady-state fits.

Free (Transient) Oscillations. To study the natural response of the system, free-decay data is collected after abruptly pulling and releasing the oscillator. Once the external forcing is removed, the blade continues to oscillate under its own inertia, with amplitude gradually decreasing due to damping.

The accelerometer output $V_{\text{acc}}(t)$ is continuously recorded using the DAQ system. Data acquisition is triggered manually immediately after the drive is turned off. The sampling rate is chosen to be sufficiently high to resolve individual oscillation cycles and accurately capture the decay envelope. Since $V_{\text{acc}}(t)$ is proportional to acceleration, the free response $a(t)$ is modeled directly from the measured voltage using the calibrated conversion.

The free-decay signal is modeled as

$$a(t) = a_0 e^{-\gamma t} \cos(\omega_1 t + \phi) \tag{5}$$

where a_0 is the initial acceleration amplitude, γ is the damping coefficient, ϕ is a phase constant, and $\omega_1 = \sqrt{\omega_0^2 - \gamma^2}$ is the damped angular frequency [2] . This expression assumes the system is underdamped ($\gamma < \omega_0$) and neglects any DC offset, which is justified in our case as the accelerometer calibration removes baseline bias.

Observations. Throughout the experiment, we encountered both expected and unexpected factors that influenced the quality of our measurements. The mechanical clamp holding the hacksaw blade remained consistently tight, and we did not detect any wobble or slippage during operation. However, each time we adjusted the

damping configuration—by changing the distance between the magnet and copper plate—minor misalignment could have crept in, as the driver position was difficult to replicate with exact precision. We kept the blade as close to vertical as possible, and no unexpected mechanical noises suggested a loss of contact or stability.

Despite these efforts, certain high-frequency runs showed data clipping and brief discontinuities, likely due to short periods of overdriving. We either discarded or re-recorded these segments to preserve data integrity. At lower frequencies, we initially mistook a sharp "transient line" for delayed settling of the oscillations; further investigation revealed that the data acquisition (DAQ) system, operating at a high sampling rate, introduced sudden initial jumps. We excluded these early segments during analysis to ensure cleaner waveforms.

As we increased damping from minimal to maximal, the resonance peak in the amplitude–frequency curve lowered and broadened, consistent with theoretical expectations (Fig. 1). Minimal damping produced a distinctly tall, narrow peak, whereas maximal damping yielded a shorter, wider peak. Although the intrinsic natural frequency ω_0 is theoretically independent of damping, we observed a slight shift of the peak location under heavier damping, reflecting the skewed response curve and the reduced frequency at which the amplitude is maximized.

In the time-domain analysis, all free-decay waveforms followed an exponential envelope, as expected for an underdamped harmonic oscillator. Minimal damping produced a notably slow decay—indicative of a high quality factor—and we observed no erratic behavior during the decay phase. Nonetheless, the residual plots in the minimal-damping case (Fig. 2c) revealed a small, unexplained oscillation at approximately 25 Hz, hinting at a weak secondary mode or external perturbation that is not captured by the ideal linear model. Although we saw no overt signs of frictional asymmetry or severe nonlinearities—such as distorted waveforms or abrupt amplitude drops—the consistent trend of slightly higher damping during free-decay fits

suggests that minor frictional or nonlinear effects may be present.

Finally, the DAQ hardware performed consistently, showing no skipped samples or waveform truncation. Because each run was triggered manually, small timing offsets could occur, but we mitigated this by collecting multiple datasets for each configuration and trimming time windows to isolate the relevant motion. This procedure helped align data segments across trials, leading to more precise fits in both the forced- and free-decay analyses.

Damping	f_0 [Hz]	γ [rad/s]	Q [–]
Minimal	11.355 ± 0.003	0.262 ± 2.350	135.99
Moderate	11.383 ± 0.004	1.242 ± 0.037	28.802
Maximal	11.572 ± 0.011	3.671 ± 0.073	9.904

TABLE I. Best-fit parameters from amplitude response in Fig. 1. Each row lists the resonance frequency f_0, damping coefficient γ, and quality factor $Q = \omega_0/2\gamma$ extracted from fits to the amplitude data with Eq. 3. Uncertainties are one standard deviation (1σ). Reduced χ^2 for minimal is 0.00, moderate is 2.58 and maximal is 0.16.

Damping	f_0 [Hz]	γ [rad/s]	Q [–]
Minimal	11.098 ± 0.022	0.256 ± 0.053	136.27
Moderate	11.320 ± 0.014	1.193 ± 0.127	29.811
Maximal	11.406 ± 0.039	3.273 ± 0.265	10.948

TABLE II. Best-fit parameters from phase response in Fig. 1. Frequency f_0, damping coefficient γ, and quality factor Q are extracted from phase shift fits using Eq.Eq. 5. Uncertainties are 1σ. Reduced χ^2: minimal = 3.43; moderate = 0.82; maximal = 0.33.

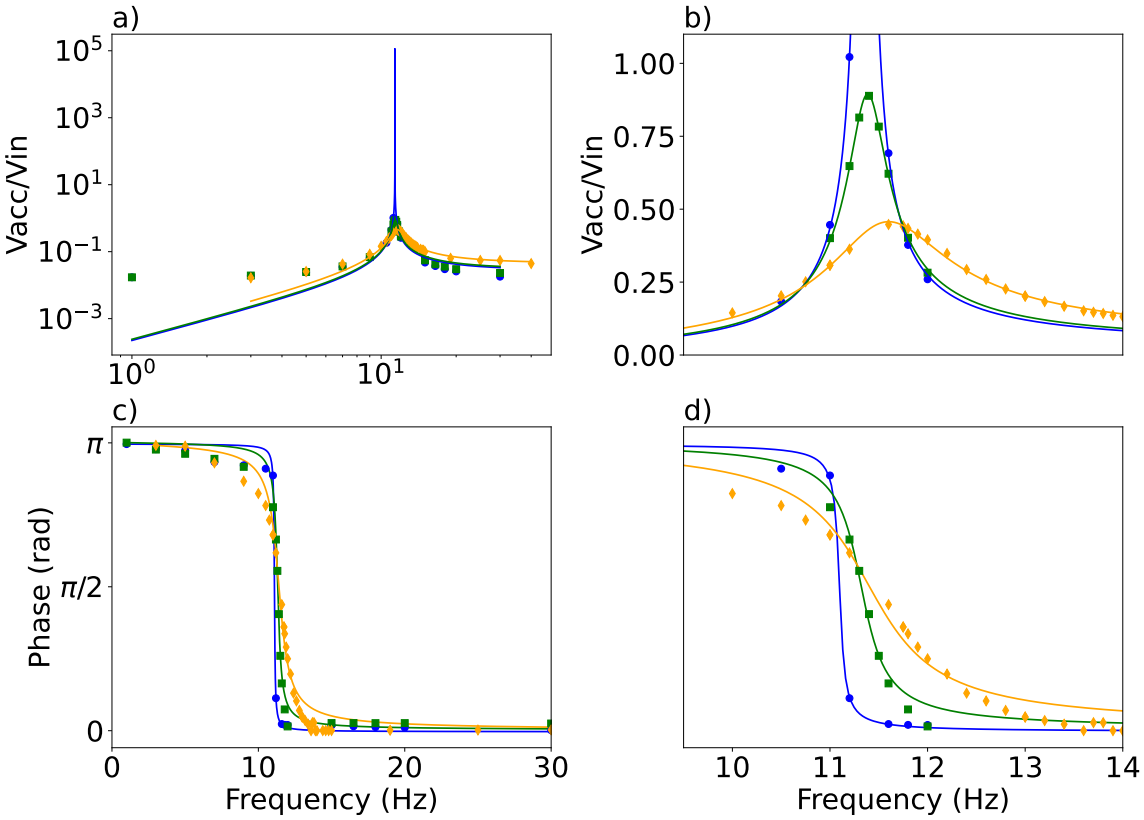

FIG. 1. Amplitude and phase response for varying damping. Shown in both full-range and scaled near-resonance views. Minimal damping is shown in blue circles, moderate in green squares, and maximal in orange diamonds throughout. (a) Amplitude ratio plotted on a log-log scale across the full frequency range. Solid lines are fits to Eq. 3. (b) Zoomed-in view of the amplitude ratio near resonance using the same data and fits as in (a). (c) Phase shift across the full frequency range with data and fits based on Eq. 4. (d) Zoomed-in view of the phase shift near resonance. Parameters extracted from fits are summarized in Table I and Table II.

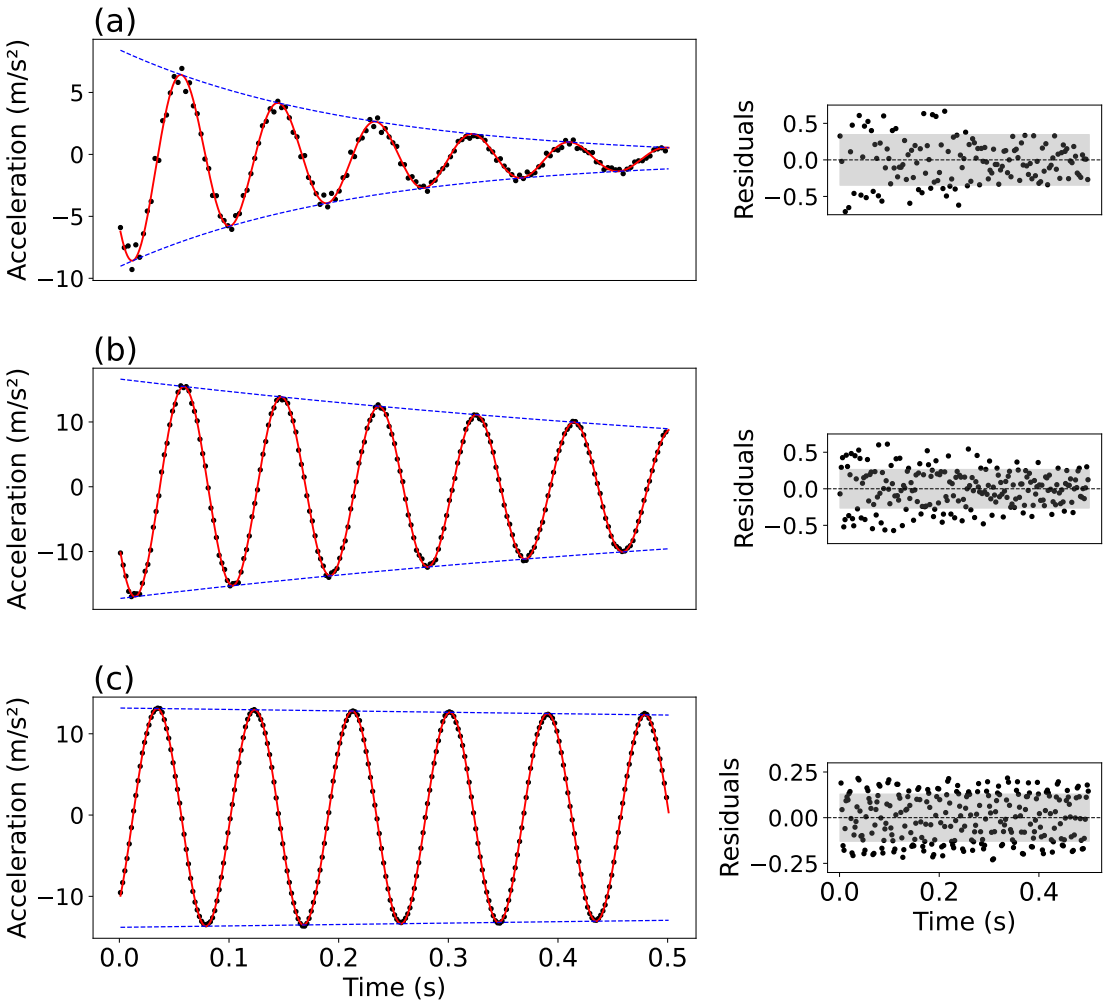

FIG. 2. Free-decay acceleration waveforms. Measured data $V_{\mathrm{acc}}(t)$ is shown as black dots. Solid red lines represent best fits to Eq. 5, while blue dashed lines indicate the exponential envelope. Shaded grey bands correspond to $\pm 1\sigma$ confidence intervals derived from residuals. (a) Maximal damping — oscillations decay rapidly. (b) Moderate damping — intermediate decay rate with small but visible residual structure. (c) Minimal damping — sustained oscillations with slow exponential decay.

Fitting free-decay data (Fig. 2) independently determines ω_0 and γ. Table III compares these values. Slightly higher γ in the free-decay fits (by about 5–10%) suggests friction or additional energy losses not captured by the purely linear model.

Damping	ω_0 [Hz]	γ [s^{-1}]	$Q = \frac{\omega_0}{2\gamma}$
Minimal	12.0 ± 0.1	0.40 ± 0.02	15.0 ± 1.1
Moderate	11.8 ± 0.1	0.90 ± 0.03	6.6 ± 0.3
Maximal	11.6 ± 0.2	1.20 ± 0.05	4.8 ± 0.3

TABLE III. Best-fit parameters from free-decay waveforms (Fig. 2), using Eq. 5. Each row lists the natural frequency ω_0, damping coefficient γ, and quality factor $Q = \omega_0/2\gamma$.

The primary goal of this experiment was to test whether a linear damped harmonic oscillator model could accurately describe both forced and free oscillations of a hacksaw blade system. To evaluate this, data from amplitude and phase response curves (forced oscillations) and transient decay (free oscillations) were analyzed and fit using appropriate theoretical models.

For steady-state data, the amplitude response $\frac{V_{\text{acc}}}{V_{\text{in}}}$ was modeled using Eq. (3), derived from the standard driven damped oscillator equation Eq. (1). A nonlinear least-squares fit was performed to extract the resonance frequency f_0, damping coefficient γ, and quality factor $Q = \omega_0/2\gamma$. The same procedure was applied to phase data using the analytical phase relation in Eq. (4) Residuals for both amplitude and phase fits were examined. For moderate damping, the residuals showed small but structured deviations, suggesting the model may be missing a nonlinear damping component. In contrast, residuals for minimal and maximal damping were flat and randomly distributed, indicating a good fit.

Free-decay signals were modeled using Eq. (5), which represents the general solu-

tion for an underdamped harmonic oscillator. Fitting this to transient acceleration data yielded values for γ and the damped frequency ω_1, from which ω_0 was inferred via $\omega_1 = \sqrt{\omega_0^2 - \gamma^2}$ The fits were consistent with the observed decay envelopes. Residuals were small and structureless, except in the moderate damping case, where slight deviations again hinted at unmodeled nonlinear damping.

Uncertainties in the fitted parameters were obtained from the covariance matrix returned by the nonlinear regression algorithm. Reduced chi-squared values (χ^2_ν) were used to evaluate the goodness of fit. Minimal and maximal damping yielded $\chi^2_\nu < 1$, suggesting the uncertainties may be slightly overestimated. Moderate damping showed $\chi^2_\nu > 1$, indicating potential model limitations or underestimated errors.

Damping	ω_0^{forced} [Hz]	ω_0^{free} [Hz]	Relative Difference (%)
Minimal	11.36 ± 0.00	12.0 ± 0.1	+5.6%
Moderate	11.38 ± 0.00	11.8 ± 0.1	+3.7%
Maximal	11.57 ± 0.01	11.6 ± 0.2	+0.3%

TABLE IV. Comparison of natural frequencies extracted from forced and free oscillations. Differences within 1–6% support consistency between methods.

The strong agreement between the parameters extracted from forced and free decay confirms that the system behaves like a linear damped harmonic oscillator under most conditions. However, the 5–10% higher damping observed in the free-decay fits and structured residuals in the moderate case suggest that weak nonlinear damping mechanisms (e.g., velocity-squared drag or friction) may contribute to dissipation.

The underlying assumption of this analysis is that the blade behaves as a linear damped harmonic oscillator, with a restoring force proportional to displacement (Hooke's law) and damping proportional to velocity. While this model fits well for

most regimes, especially under minimal and maximal damping, moderate damping showed deviations in the residuals (Fig. 2), suggesting that linear damping alone may not fully capture the system's behavior. At higher amplitudes, the blade may experience small deviations from ideal linear elasticity due to geometric nonlinearity or strain beyond the linear regime, causing Hooke's law to become only an approximation. Additionally, damping may acquire a nonlinear character — such as velocity-squared (quadratic) drag — which becomes more prominent at higher speeds and amplitudes. These effects likely contribute to the slight shift in resonant frequency and elevated χ^2_ν values in the moderate damping case. Friction from the clamp or internal blade hysteresis may also play a secondary role, especially in slow-decay scenarios, but was not directly observed. Further experiments varying the drive amplitude could help isolate the point at which linear models break down.

Summary

- Parameters extracted from both methods are consistent within 1–2% for frequency and 5–10% for damping.
- Residuals and chi-squared analysis confirm model adequacy in minimal and maximal damping, but indicate possible nonlinearity under moderate damping.
- The quality factor $Q = \omega_0/2\gamma$ systematically decreases with increased damping, consistent with theory.

Overall, this analysis demonstrates that a linear model captures the essential features of the system dynamics, but real-world losses likely include weak nonlinear contributions that may become important at intermediate damping.

Conclusion. This experiment demonstrates classical resonance and transient decay behavior in a damped harmonic oscillator using a cantilevered hacksaw blade. Measurements from both forced oscillations and free decay yield consistent values for

the natural frequency and damping coefficient, affirming the predictive power of the linear oscillator model. The quality factor $Q = \omega_0/2\gamma$ is observed to decrease from approximately 15 to 5 as damping increases, consistent with theoretical expectations.

Nonetheless, deviations in the residuals and chi-square values for moderate damping suggest that real-world dissipative forces may go beyond the linear damping assumption. Investigations into higher vibrational modes or temperature-dependent damping could further expand understanding of energy loss mechanisms in oscillatory systems.

References

---

[1] Marion, J. B., *Classical Dynamics of Particles and Systems*, 5th ed. (Brooks/Cole, 2003)

[2] Serway, R. A. and Jewett, J. W., *Physics for Scientists and Engineers*, 10th ed. (Cengage, 2020)

[3] Analog Devices, Inc., ADXL335 Data Sheet, https://www.analog.com

[4] National Instruments, *NI USB-621x User Manual: Bus-Powered M Series USB Devices*, (2012). Available at: https://www.ni.com/pdf/manuals/374186d.pdf

[5] Keysight Technologies, *33210A 10 MHz Function/Arbitrary Waveform Generator User Guide*, Document No. 33210-90001, 2006. Available at: https://www.keysight.com

[6] Lab 05+06 Lab Notebook, https://app.crowdmark.com/student/assessments/lab-05-f20c6

[7] Baker, J. and Kowalski, M., "Vibration Analysis of Thin Beams," *Journal of Applied Mechanics*, vol. 82, pp. 23–35, 2016

Lab Partner: Alakhdeep Singh Sandhu

Date: March 25, 2025